Runx3 is required for oncogenic Myc upregulation in *p53*−deficient osteosarcoma

Shohei Otani[1,2†], Yuki Date[1,3†], Tomoya Ueno[1], Tomoko Ito[1], Shuhei Kajikawa[4], Keisuke Omori[1,2], Ichiro Taniuchi[5], Masahiro Umeda[2], Toshihisa Komori[6], Junya Toguchida[7,8], and Kosei Ito[1*]

1. Department of Molecular Bone Biology, Graduate School of Biomedical Sciences, Nagasaki University, 1-7-1 Sakamoto, Nagasaki, 852-8588, Japan.

2. Department of Clinical Oral Oncology, Graduate School of Biomedical Sciences, Nagasaki University, 1-7-1 Sakamoto, Nagasaki, 852-8588, Japan.

3. Japan Society for the Promotion of Science, 5-3-1 Kojimachi, Chiyoda-ku, Tokyo, 102-0083, Japan.

4. Department of Veterinary Medicine, Faculty of Veterinary Medicine, Okayama University of Science, 1-3 Ikoinooka, Imabari, Ehime, 794-8555, Japan.

5. Laboratory for Transcriptional Regulation, RIKEN Center for Integrative Medical Sciences, 1-7-22, Suehiro-cho, Tsurumi-ku, Yokohama, 230-0045, Japan.

6. Department of Cell Biology, Graduate School of Biomedical Sciences, Nagasaki University, 1-7-1 Sakamoto, Nagasaki, 852-8588, Japan.

7. Institute for Frontier Life and Medical Sciences, Kyoto University, Shogoin-Kawahara-cho, Sakyo-ku, 606-8507 Kyoto, Japan.

8. Center for iPS Cell Research and Application (CiRA), Kyoto University, 53 Shogoin-Kawahara-cho, Sakyo-ku, 606-8507 Kyoto, Japan.

[†]These authors contributed equally.

[*]Corresponding author. E-mail: itok@nagasaki-u.ac.jp

Running title; Oncogenic Runx3−Myc axis in *p53*-deficient osteosarcoma

Abstract

Osteosarcoma (OS) in human patients is characterized by genetic alteration of *TP53*. Osteoprogenitor-specific *p53*-deleted mice (*OS* mice) have been widely used to study the process of osteosarcomagenesis. However, the molecular mechanisms responsible for the development of OS upon p53 inactivation remain largely unknown. In this study, we detected prominent RUNX3/Runx3 expression in human and mouse *p53*-deficient OS. Myc was aberrantly upregulated by Runx3 via mR1, a consensus Runx site in the *Myc* promoter, in a manner dependent on *p53* deficiency. Reduction of the Myc level by disruption of mR1 or Runx3 knockdown decreased the tumorigenicity of *p53*-deficient OS cells and effectively suppressed OS development in *OS* mice. Furthermore, Runx inhibitors exerted therapeutic effects on *OS* mice. Together, these results show that *p53* deficiency promotes osteosarcomagenesis in human and mouse by allowing Runx3 to induce oncogenic Myc expression.

Introduction

TP53 is the most frequently mutated gene in all types of human cancer, with mutations present in more than half of all tumors, and alteration of p53 that leads to loss of wild-type p53 activity is a master driver in most cancers[1–3]. Accordingly, p53 is one of the most intensively studied tumor suppressor proteins. *p53*-null mice develop tumors at high penetrance, and *p53*-deficient mice crossed with mouse lines in which other cancer-related genes have been targeted have been widely used to elucidate the mechanisms of human cancer development. However, the diversified functions of p53 and the disparate consequences of its disruption prevent us from understanding the nature of *p53*-deficient carcinogenesis.

Osteosarcoma (OS) is the most common malignant bone tumor[4]. Patients with germline mutations in *TP53* (Li-Fraumeni syndrome) have a high incidence of OS[5,6], and *TP53* inactivation is often detected in sporadic OS[4,7]. In mice, restrictive deletion of *p53* in osteoprogenitor and mesenchymal stromal cells (MSCs) leads to development of OS with close histopathological resemblance to human OS, e.g., in the *Osterix (Osx)/Sp7*-Cre; *p53*^{fl/fl} mouse line, which is widely used as an animal model of human OS[8,9]. Thus, loss of p53 is a predominantly critical 'solo-driver' of osteosarcomagenesis in both human and mouse. Therefore, the scrutiny of *p53*-deficient osteosarcomagenesis should provide molecular insights into the universal mechanisms of tumorigenesis and malignancy caused or triggered by *p53* deficiency. Currently, however, little is known about the molecular events that result from loss of p53 and lead to OS development.

Dysregulation of transcription factors (TFs) plays pivotal roles in multiple cancers[10]. Focusing on changes in the expression of genes encoding TFs, we compared the transcriptome of *p53*-deficient OS tissues to that of normal (wild-type) osteoblasts in human and mouse. Runx3, a member of the Runx family of genes, was the most upregulated TF in the absence of p53; c-Myc (Myc) and AP1 TFs, which have been attracted attention as oncogenes in OS[4,11,12], were also upregulated. Subsequent

comprehensive genome-wide analyses revealed that Runx3 directly upregulates Myc in the *p53*-null context.

Our findings demonstrate that Runx3 functions as an oncogene to upregulate Myc via mR1, a genome element found in the *Myc* promoter; consistent with this, Runx inhibitors are efficacious against *p53*-deficient osteosarcomagenesis *in vivo*. Based on our findings, we propose that tumorigenesis driven by *p53* deficiency intrinsically requires the Runx3–Myc oncogenic axis.

Results

Runx3 is highly upregulated and oncogenic in p53-deficient OS in human and mouse

p53 inactivation is critical for osteosarcomagenesis in both human and mouse. Almost all OS patients (85 of 86) in the Therapeutically Applicable Research to Generate Effective Treatments (TARGET) cohort possessed *TP53* alterations: 84 had *TP53* genetic alterations, and one had *MDM2* amplification (Fig. 1A). *Osterix (Osx)/Sp7*-Cre; *p53*^fl/fl mice (herein *OS* mice) frequently developed OS as reported[8,9] (Supplementary Fig. 1A). We compared the transcriptome of human or mouse OS tissues to that of normal osteoblasts or newborn calvaria, respectively (Supplementary Fig. 1B), focusing on changes in the expression of genes encoding 794 human TFs and 741 mouse orthologues. This analysis identified 47 TFs that were commonly up or downregulated more than 2-fold in human and mouse OS (Supplementary Table 1). Seven of the top ten TFs (shown in blue; Fig. 1A and B), when ranked by expression level, had orthologues in both species (Supplementary Fig. 1C). Among these seven TFs, *RUNX3* was associated with portended poor prognosis in human OS (Supplementary Fig. 1D). Moreover, *RUNX3* was over-expressed in almost every human and mouse OS; the highest degree of upregulation ($\log_2$FC) was 5.0 and 2.2 in human and mouse, respectively (Fig. 1A, B). A similar, though less pronounced, trend was also observed for *MYC*, *JUNB*, and *FOS*. These observations inspired us to investigate the oncogenic roles of RUNX3/Runx3 in OS development.

RUNX3, a member of the RUNX family of genes, is a cancer-related TF[13]. In contrast to the other members of the family, RUNX1 and RUNX2, and their subunit CBFβ, RUNX3 was markedly upregulated in both human (Fig. 1A) and mouse OS (Fig. 1B and Supplementary Fig. 2A). We isolated tumor cells from *OS* mice (mOS cells) and assessed their tumorigenic potential in immunocompromised mice (Supplementary Fig. 2B). mOS cell clones manifesting strong tumorigenicity were associated with aberrant Runx3 expression (Supplementary Fig. 2C) and recapitulated the histology of primary tumors (Supplementary Fig. 2D), in which Runx3 was specifically immunodetected in Runx2-positive osteogenic cells (Supplementary Fig. 2E). The positive correlation between

tumorigenicity and RUNX3 expression was also observed in a series of human OS cells (Supplementary Fig. 3A). RUNX3/Runx3 knockdown decreased tumorigenicity in all human and mouse OS cells tested to a greater extent than knockdown of RUNX2/Runx2 (Supplementary Fig. 3B-E). RUNX1/Runx1 expression had no significant effect upon osteosarcomagenesis (Fig. 1A; Supplementary Fig. 2A, C; Supplementary Fig. 3A), and its knockdown did not affect the tumorigenicity of OS cells (Supplementary Fig. 3B). Together, these results indicate that Runx3 is required for the tumorigenicity of *p53*-deficient OS cells. Although Rb inactivation potentiates *p53*-deficient OS development[8], there was no explicit association between inactivation of Rb and tumorigenicity of mOS cells (Supplementary Fig. 2C).

We depleted *Runx3* from *OS* mice. Between the two independent promoters of *RUNX3/Runx3*[14], P1 and P2, *Runx3(P1)* was expressed several times more strongly than *Runx3(P2)* in mouse OS (Supplementary Fig. 4A). *OS* mice with heterozygous *Runx3* deletion in osteoprogenitors (*OS*; *Runx3*$^{fl/+}$) or systemic null mutation of *Runx3(P1)* (*OS*; *Runx3(P1)*$^{\Delta/\Delta}$) (Supplementary Fig. 4B-F) exhibited improvement in OS incidence and lifespan, mirroring the reduction of Runx3 expression in bone marrow (BM)-MSCs (Fig. 1C-E). However, many *OS*; *Runx3*$^{fl/fl}$ mice (*OS* mice lacking both *Runx3(P1)* and *Runx3(P2)* in osteoprogenitors) died before OS development (Supplementary Fig. 5D-F), probably due to loss of the pro-proliferation function of Runx3[15]. By contrast, homozygous or heterozygous deletion of *Runx1* had little effect on lifespan and OS incidence in *OS* mice (Supplementary Fig. 5A, B). *OS* mice with heterozygous deletion of *Runx2* (*OS*; *Runx2*$^{fl/+}$), which is essential for osteoblast differentiation[16], died early before OS onset (Supplementary Fig. 5C-F). Taken together, these results highlight the oncogenic roles of RUNX3/Runx3 in *p53*-deficient osteosarcomagenesis in human and mouse.

Myc is a positive target of Runx3 in p53-deficient OS

To explore the target genes of Runx3 in *p53*-deficient OS cells, we investigated the genome-wide profiles of Runx3 and open and active chromatin using ChIP-seq of Runx3 and H3K27ac and assay for transposase-accessible chromatin using sequencing (ATAC-

seq) (Fig. 2A) in a representative mOS cell line that exhibits Runx3-dependent tumorigenicity (Supplementary Fig. 3A). Genome-wide binding of Runx3 and open/active chromatin were highly concordant, with 1,624 genes strongly co-occupied by both Runx3 and accessible chromatin markers (or open/active chromatin), indicating that Runx3 acts as a general transcriptional activator in OS cells (Fig. 2A; Supplementary Fig. 6A, B). In addition, we used microarrays to investigate changes in the transcriptome upon *Runx3(P1)* knockout in *p53*-null BM-MSCs; this analysis identified 1,552 potential targets upregulated by Runx3(P1) (Fig. 2B). Of the 95 genes shared between the 1,624 Runx3-occupied and 1,552 Runx3-upregulated genes (Supplementary Fig. 6C; Supplementary Table 2), *c-Myc* (*Myc*) was most strongly occupied by Runx3 and open/active chromatin within its regulatory region (Fig. 2A; Supplementary Table 2); moreover, this gene was among the factors most strongly associated with poor prognosis (Supplementary Fig. 6D). Changes in Myc-target-gene expression were enriched in *p53*-deficient human and mouse OS (Supplementary Fig. 6E, F), and loss of Runx3(P1) reversed this enrichment (Supplementary Fig. 6G). Thus, we identified Myc as the top candidate target gene upregulated by Runx3 in *p53*-deficient OS cells.

Myc, which is crucial for OS development[17], was markedly upregulated in human and mouse OS (Fig. 1A and B). Among the RUNX family genes, the expression of *RUNX3/Runx3* was most strongly correlated with that of *MYC/Myc* in both human and mouse OS (Fig. 2C). Runx3 and Myc expression were highly correlated in terms of protein levels (Supplementary Fig. 7A) in mOS cells and localization in OS tissues (Supplementary Fig. 7B, C). In human and mouse OS cells, knockdown of RUNX3/Runx3 led to down-regulation of MYC/Myc, whereas overexpression led to upregulation (Supplementary Fig. 7D-F). Moreover, MYC/Myc was required for tumorigenicity (Supplementary Fig. 7G, H). Importantly, heterozygous deletion of *Myc* greatly prolonged the lifespan and reduced OS incidence of *OS* mice (Fig. 2D, E), as was the case for *Runx3* (Fig. 1D, E). *OS* mice with homozygous deletion of *Myc* (*OS*; *Myc*$^{fl/fl}$) died early before OS onset, as did *OS*; *Runx3*$^{fl/fl}$ mice (Supplementary Fig. 5D-F). Overall, the oncogenic effects of Myc and Runx3 were highly concordant in *p53*-deficient osteosarcomagenesis *in vivo*.

The mR1 element is responsible for Myc upregulation by Runx3

To identify the elements within its 3-megabase (Mb) topologically associating domain (TAD) (27) (Fig. 3A) through which Runx3 upregulates *Myc*, we performed CRISPR-interference (CRISPRi)[18], in which chromatin is repressed by dCas9-KRAB in a targeted manner. For this analysis, we chose candidate elements with high levels of co-occupancy of Runx3 and open/active chromatin, as well as high conservation across mammals (Fig. 3A). The transcription start site (TSS) and leukemic enhancers N-Me and BDME of *Myc*[19] were also included as controls. Blockage of mR1, a consensus Runx site located ~0.36 kb upstream of TSS, exhibited a significant reduction in Myc expression, comparable to the effect observed at the TSS in mOS cells (Fig. 3B, C). None of the CRISPRi trials affected expression of *Pvt1*, a neighboring lncRNA that regulates *Myc*[20] (Fig. 3A, C). All three RUNX consensus sites (MR1/mR1, MR2/mR2, and MR3/mR3) in the *MYC*/*Myc* promoter (Supplementary Fig. 8A) were bound by RUNX2/Runx2 and RUNX3/Runx3, but not RUNX1/Runx1 (Supplementary Fig. 8B-F). Among them, only MR1/mR1 is in a region that is well conserved between human and mouse (Supplementary Fig. 8A). Consistent with this, blockage of only mR1 decreased the tumorigenicity and Myc expression level of mOS cells (Fig. 3E, F), even though mR3 was predominantly bound by Runx3 (Fig. 3D; Supplementary Fig. 8B, C).

To investigate the roles of mR1 with greater precision, we used genome editing to generate mutant mOS cell clones in which mR1 was homozygously disrupted (Fig. 3G). Depending on the degree of mR1 mutation that inhibited Runx2/3 binding, Myc expression and tumorigenicity of mOS cells were reduced (Fig. 3G-J), as was also observed in another mOS cell line (Supplementary Fig. 9B) and human OS SJSA1 cells (Supplementary Fig. 9D). Deletion of a few bases neighboring mR1 or deletion of mR3 had little effect, although substitution of a single nucleotide within mR1 had a significant effect (Supplementary Fig. 9A, C, E, F), confirming that mR1 was specifically required for oncogenicity. A mR1 mutation specifically inhibited entry of RNA polymerase II at the P2 promoter, from which the majority of *Myc* transcripts are derive[21], in mOS cells (Fig. 3K).

mR1 and Runx3 are responsible for development of OS in p53-deficient mice

To evaluate the roles of mR1, mR2, and mR3 roles in mice, we replaced each of these sequences with a size-matched 6 bp *BglII* site using genome editing (Supplementary Fig. 10E, H, I); mR1 was mutated using both homologous recombination and genome editing to ensure reproducibility (Supplementary Fig. 10A-C, E). Mice harboring these mutations were crossed with *OS* mice (Supplementary Fig. 10D). Homozygous disruption of mR1, but not of mR2 or mR3, abolished Myc upregulation in BM-MSCs of *OS* mice (Fig. 4A). Regardless of how the mice were generated, homozygous disruption of mR1 (*OS*; *mR1*$^{m/m}$) improved the lifespan and OS incidence of *OS* mice, whereas mutation of mR2 (*OS*; *mR2*$^{m/m}$) or mR3 (*OS*; *mR3*$^{m/m}$) did not have such a tumor-suppressive effect (Fig. 4B and C; Supplementary Fig. 10F, G, J, K). In fact, *OS*; *mR1*$^{m/m}$ mice were nearly identical to *OS*; *Runx3*$^{fl/+}$ mice in terms of survival and OS incidence (Fig. 4D, E). Together, these results clearly show that in a *p53*-deficient setting, Runx3 upregulates Myc via mR1 to promote OS development.

For further confirmation of the Runx3 oncogenicity, *OS* mice were treated with the Runx inhibitors, Ro5-3335[22] and AI-01-104[23], which inhibit the interaction between Runx and Cbfβ, thereby inhibiting Runx transactivation. Administration of either of these compounds effectively prolonged the lifespan of *OS* mice after the onset of OS (Fig. 4F)

Induction of Myc by Runx3 is dependent on p53 deficiency

In the absence of p53, disruption of either mR1 or Runx3(P1) prevented upregulation of Myc in BM-MSCs (Fig. 4A; Fig. 5B). On the other hand, in the presence of p53, neither disruption of mR1 nor disruption of Runx3(P1) affected Myc expression, which was expressed at a low basal level in BM-MSCs (Fig. 5A, B). Interestingly, restoration of p53 significantly decreased Myc upregulation in *p53*-negative BM-MSCs, but did not reduce expression below the basal level of expression that was retained in the absence of Runx3 (Fig. 5C). Likewise, Myc was efficiently downregulated by p53 induction in mOS cells, but not in *Runx3*-negative mOS cells derived from OS that occasionally developed in *OS;*

Runx3^{fl/fl} mice (Supplementary Fig. 11A-C). Therefore, Runx3 upregulates Myc via mR1 only in the *p53*-negative context.

In human OS cells, exogenous RUNX3 induced MYC in *p53*-negative G292 cells but not in *p53*-positive U2OS cells (Supplementary Fig. 11D). Notably, two p53 mutants expressed in HOS/MNNG-HOS/143B (R156P)[24] and NOS-1 (R273H) cell lines (Supplementary Fig. 11E) failed to repress Myc (Fig. 5D; Supplementary Fig. 11F). Importantly, although Runx3 directly interacted with wild-type p53, as previously reported[25], both p53 mutants lost their interaction with Runx3 (Fig. 5E) and the ability to suppress Runx3 transcriptional activity (Fig. 5F). Consistent with this, MNNG-HOS and NOS-1 cells exhibited RUNX3-dependent MYC regulation (Supplementary Fig. 7F). These results suggest that p53 prevents Myc upregulation by physically inhibiting Runx3.

Next, we performed EMSA to determine whether p53 affects Runx3 ability to bind mR1. In these experiments, we used *p53*-negative mOS cells and other *p53*-positive murine cell lines: ST2 (a BM-MSC line) and 3T3-E1 (an osteoblast progenitor line). To quantitatively compare the amounts of endogenous Runx proteins, we utilized a pan-Runx monoclonal antibody that evenly reacted with all Runx proteins by recognizing the conserved C-terminal VWRPY motif (Supplementary Fig. 12A-C). In ST2 and 3T3-E1 cells, both of which were *p53*-positive, the amount of mR1-bound Runx3 was smaller than in *p53*-negative mOS cells, and inversely proportional to the amount of endogenous p53 (Supplementary Fig. 12C-E). This observation implies that p53 inhibits Runx3 DNA binding. The amount of mR1-bound Runx2, on the other hand, was constant and less strongly affected by the presence of p53 (Supplementary Fig. 12C-E). In fact, the amount of Runx3 bound to mR1 was reduced by either addition of p53 (Supplementary Fig. 12F) or induction of p53 in mOS cells (Supplementary Fig. 12G), whereas the amount of bound Runx2 was unaffected. Consistent with these results, p53 exhibited a stronger interaction with Runx3 than with Runx2, both exogenously and endogenously (Supplementary Fig. 12H, I), and more effectively attenuated the transcriptional activity of Runx3 than that of Runx2 (Supplementary Fig. 12J).

RUNX2 reportedly promotes development of OS[13,26–28]. To assess the function of this protein, we examined *Runx3*-negative mOS cells and observed both Runx2- and mR1-dependent tumorigenicity. In these cells, the level of Myc correlated well with that of Runx2 (Supplementary Fig. 13A), and knockdown of Runx2 decreased both Myc expression and tumorigenicity (Supplementary Fig. 13B). In this *Runx3*-negative context, Runx2 bound to mR1 (Supplementary Fig. 13C-E), which was responsible for Myc upregulation and tumorigenic potential in these cells (Supplementary Fig. 13F, G), whereas Runx1 exhibited neither correlation with Myc expression nor occupancy of mR1 (Supplementary Fig. 13A, C-E). Thus, Runx2 compensated for Runx3 in osteosarcomagenesis, and in OS cells with weaker Runx3 oncogenicity or more normal p53 activity, the pro-tumorigenic activity of Runx2 is more pronounced.

The Runx inhibitor, AI-01-104 decreased Runx3-enhanced Myc expression in *p53*-negative mOS cells, but did not affect the basal physiological level of Myc in *p53*-positive ST2 cells (Fig. 5G). The ability of Runx inhibitors to repress Myc was specific to the *p53*-deficient context, clearly demonstrating that induction of Myc by Runx3 is dependent on *p53* deficiency (Fig. 5H).

Discussion

p53-deficient osteosarcomagenesis was inhibited by reduction of Myc or Runx3, disruption of mR1, or administration of Runx inhibitors, demonstrating that a key feature of *p53*-deficient osteosarcomagenesis is the aberrant upregulation of Myc by Runx3 via mR1. We did not address the mechanism of Runx3/Runx3 upregulation. However, p53 may indirectly repress Runx3 via miRNAs because p53 indirectly modulates miRNA repression of Runx2 (which is released from repression in the absence of p53)[29]. Additionally, it is reasonable to assume that oncogenic signaling pathways in the *p53*-deficient tumor microenvironment play important roles in the Runx3 upregulation. TGF-β signaling strongly induces oncogenic Runx3 upregulation in *p53*-deficient pancreatic ductal adenocarcinoma [30], in which Myc functions as a critical oncogene[31]. Expression of Runx3 and of Myc may also form a positive regulatory loop[32].

The tumor-suppressive function of RUNX3 initially attracted attention based on observations of gastric phenotypes in *Runx3*-deficient mice and the causal relationship between *RUNX3* silencing and the genesis of human gastric cancer[33]. In a diverse range of human cancers, including gastric, colorectal, lung, pancreas, breast, liver, and prostate cancers, as well as leukemia and neuroblastoma, RUNX3 inactivation occurs mainly due to hypermethylation of the promoter or protein mislocalization[13,34]. More recently, on the other hand, RUNX3 upregulation has been also observed in various cases of human malignant tumors, suggesting its oncogenic roles[13,35]. Importantly, RUNX3 facilitates the growth of Ewing sarcoma cells[36]. Over the past two decades, research on RUNX3 further revealed its tumor-suppressive or oncogenic functions, bringing sharper focus on a fundamental question; how are the dualistic roles of RUNX3 determined by cellular context? Given the potential medical value of targeting RUNX transcriptional activities[22,37,38], the demand to answer this question is growing. The results presented indicate that p53 status is a contextual determinant of the dual roles of RUNX3[39]. p53 inactivation is the crucial event responsible for Runx3 oncogenicity leading to development of OS. In fact, in *p53*-positive U2OS cells (Supplementary Fig. 11D), elevated levels of

RUNX3 induced p21 expression (data not shown), highlighting the fact that RUNX3 can play a tumor-suppressive role by promoting transactivation of wild-type p53, as previously reported[25].

As with loss of p53, MYC activation has been observed in more than half of all cancers; Myc directly contributes to malignant transformation through its pathogenic roles in tumor initiation, progression, and maintenance[40]. *Myc* is critically regulated by tissue-specific regulatory regions, underscoring the fundamental importance of cancer-specific enhancers/superenhancers, and making *Myc* gene the best example thus far of long-range regulation. However, the fundamental mechanisms driving enhancer–promoter transactivation remain unclear[41], probably because the available evidence regarding TFs responsible for the transactivation remains inadequate. Under these circumstances, identification of mR1, a promoter element that is essential for aberrant upregulation of *Myc*, can provide deeper insight into the enhancer–promoter regulation of *Myc*. Given that Runx3 is a general and genuine transcriptional activator of Myc in the absence of p53, and that Runx1 is involved in *Myc* regulation via superenhancers[19], Runx3 may function as a crucial modulator to activate the superenhancer/core promoter of *Myc* in concert with other transcription factors such as Smads[30] and AP1, both of which interact with Runx proteins[42]. AP1 TFs are prominently upregulated in human and mouse OS (Fig. 1A, B), and, interestingly, consensus motifs of AP1 and Runx are co-enriched genome-wide (Supplementary Fig. 6B). Further studies should seek to determine whether depletion of Runx consensus sites in superenhancer candidates suppresses tumorigenesis in animal cancer models.

RUNX2 contributes to OS formation, and RUNX2 expression associates with p53 expression and MYC expression in human OS cells. RUNX2 mediates epigenetic changes to maintain MYC expression in OS[27]. We show that RUNX3/Runx3 is more strongly induced than RUNX2/Runx2 in human and mouse *p53*-deficient OS (Fig. 1). We also show that p53 binds to Runx3 more strongly than to Runx2 (Supplementary Fig. 12), and that Runx3 upregulates Myc only in the absence of p53 (Fig. 5). Furthermore, the oncogenic activity of Runx2 is more pronounced in OS cells with weaker Runx3 oncogenicity,

suggesting that the oncogenicity of Runx3 is supplemented by Runx2 (Supplementary Fig. 13). Taken together, these findings suggest that Runx3 is mainly responsible for Myc upregulation caused by p53 loss. Either Runx2 or both Runx2 and Runx3 contribute to Myc upregulation and probably maintain aberrant Myc expression levels by epigenetic dysregulation.

p53 deficiency and Myc excess, two major forces governing genesis and progression of most cancers in humans and mouse, are linked through Runx3 and mR1, providing a rationale for the targeting of Runx3 in cancer therapy. p53 is not amenable to pharmacological manipulation and has been widely deemed to be 'undruggable'[43]. Instead of direct retrieval of p53, indirectly targeting Runx3 or mR1 using drugs that inhibit the interaction of Runx and Cbfβ[22,23] as shown in this study (Fig. 4F), or PI polyamides targeting the consensus RUNX-binding sequences[38] could effectively achieve the same goal. The oncogenic Runx3–Myc axis is most likely to be critical for *p53*-deficient malignancies other than OS. The AI-10-104 dose we used (Fig. 4F) did not affect wild-type mice weights, showing little effect on physiological status (data not shown). Because this oncogenic axis is dormant in *p53*-proficient normal cells (Fig. 5H), it is an attractive and widely applicable target for anti-tumor pharmacotherapy in a variety of human cancers, in particular from the standpoint of avoiding side effects.

Materials and methods

Mouse lines

Floxed mouse lines of *Runx1*[44], *Runx2*[45], *Runx3*[46], *p53*[47], and *Myc*[48] were described previously. The *Sp7/Osx*-Cre line (no.006361) was purchased from Jackson Laboratory. All mouse studies were performed in the C57BL/6 background, using approximately equal numbers of males and females.

　　　The details of all animal experiments, including the number of mice (sample size) to be used, were reviewed and approved by the Animal Care and Use Committee of Nagasaki University Graduate School of Biomedical Sciences (no. 1603151292‐ 14). Four mice were housed in each cage. Mice were reared in a pathogen‐ free environment on a 12-hour light cycle at $22 \pm 2^{\circ}$C.

ChIP-qPCR and ChIP-seq

ChIP experiments were performed using the SimpleChIP Enzymatic Chromatin IP kit with magnetic beads (Cell Signaling Technology). Briefly, 6 million cells were cross-linked with 1% formaldehyde for 10 min at room temperature. After permeabilization, cross-linked cells were digested with micrococcal nuclease and immunoprecipitated with isotype control, anti-Runx3 (D6E2; Cell Signaling Technology), anti-H3K27ac (D5E4; Cell Signaling Technology), or anti-RNAPII subunit B1 (Rpb1) NTD (D8L4Y; Cell Signaling Technology) antibodies. Immunoprecipitated products were isolated with Protein G Magnetic Beads (Cell Signaling Technology) and subjected to reverse cross-linking. The DNA was subjected to quantitative PCR using the primer pairs listed in Supplementary Table 3.

　　　For high-throughput sequencing, libraries were prepared using the NEBNext Ultra II DNA Library Prep Kit for Illumina, and then purified with AMPure XP beads. Libraries were sequenced on the Illumina HiSeq platform.

ATAC-seq

ATAC-seq experiments were performed as described[49]. Briefly, 50,000 cells were washed with PBS and lysed in lysis buffer (10 mM Tris-HCl, 10 mM NaCl, 3 mM $MgCl_2$, 0.1% Igepal CA-630). Transposed DNA fragments were generated using the Tagment DNA TDE1 Enzyme and Buffer Small Kit (Illumina), and amplified by PCR with an additional two cycles relative to the original protocol[49] using NEBNext High-Fidelity 2× PCR Master Mix (New England Biolabs). ATAC-seq libraries were sequenced on the Illumina HiSeq platform.

Analysis of ChIP-seq and ATAC-seq

Reads were trimmed of adapter sequences using fastp[50] and aligned to the mouse genome (mm10) using bowtie2[51]. After removal of PCR duplicates with Picard MarkDuplicates (http://broadinstitute.github.io/picard), peaks were called using the findPeaks function of HOMER[52] (http://homer.ucsd.edu/homer) with the input set as a control. Correlations between ChIP-seq and ATAC-seq samples were calculated using the plotCorrelation function of deepTools[53]. De novo motif prediction was performed using the findMotifs functions of HOMER with default settings. All peaks of ATAC-seq and ChIP-seq samples were merged and partitioned into three clusters according to the scores calculated by the mergePeaks feature of HOMER[52]. Along the positions of the merged peaks, heatmaps were drawn using the plotHeatmap function of deepTools. The 1624 genes nearest the peaks detected in the strongly co-occupied cluster were considered significant. Topologically associating domain (TAD) boundaries for *Myc* were determined by referring to previously used[54].

Epigenome editing

HEK293T cells were cotransfected with individual sgRNA-dCas9-KRAB lentiviral expression plasmids (#71236; Addgene), the second-generation packaging plasmid psPAX2 (#12260; Addgene), and the envelope plasmid pMD2.G (#12259; Addgene) by a standard lipofection method. After filtration with a 0.45-µm filter, c, conditioned medium containing lentivirus was used for transduction. Transduced cells were selected with puromycin. Expression of FLAG-tagged dCas-KRAB in mOS1-1 cells was immunodetected using an anti-FLAG antibody (M2). sgRNA sequences are listed in Supplementalry Table S4.

Administration of Runx inhibitors

OS mice that developed OS in the lower limbs, the most frequent site, were selected blindly, and administration of the inhibitors via intraperitoneal injection was initiated when the onset of OS was visually confirmed (i.e., when the tumor was around 3 mm in diameter). Ro5-3335 or AI-10-104 were administered at 5 mg/kg in 100 µl of 50% DMSO in PBS or 1 mg/kg in 100 µl of 10% DMSO in PBS, respectively, once every 3 or 4 days (twice a week) for 10 weeks after OS onset.

Statistics

All quantitative data are expressed as means ± SD. Differences between groups were calculated by unpaired two-tailed Student's t-test for two groups or by one-way analysis of variance (ANOVA) for more than two groups. All analysis was performed in Prism 8 (GraphPad software). Survival was analyzed by the Kaplan–Meier method and compared by the log-rank test using the same software. $p<0.05$ denotes significance. No samples from *in vivo* and *in vitro* experiments were excluded from the analysis.

Data and materials availability

All data are available in the main text or the supplementary materials. The ChIP-seq/ATAC-seq and RNA-seq data generated in this study were submitted to DDJB sequence read archive (DRA) with accession numbers DRA009517 and DRA011168, respectively.

Author contributions: K.I. initiated the study. Y.D. and K.I. designed the experiments. S.O., Y.D., T.U., T.I, S.K., K.O., J.T., and K.I conducted the experiments. Y.D. performed bioinformatic analyses. I.T. and T.K. generated and provided animal materials. S.O, Y.D., and K.I. wrote the manuscript. M.U. and T.K. coordinated the project. K.I supervised the study.

Competing interests

The authors declare no competing interests.

References

1 Lawrence MS, Stojanov P, Mermel CH, Robinson JT, Garraway LA, Golub TR *et al.* Discovery and saturation analysis of cancer genes across 21 tumour types. *Nature* 2014; **505**: 495–501.

2 Bouaoun L, Sonkin D, Ardin M, Hollstein M, Byrnes G, Zavadil J *et al.* TP53 Variations in Human Cancers: New Lessons from the IARC TP53 Database and Genomics Data. *Hum Mutat* 2016; **37**: 865–876.

3 Muller PAJ, Vousden KH. Mutant p53 in Cancer: New Functions and Therapeutic Opportunities. *Cancer Cell* 2014; **25**: 304–317.

4 Kansara M, Teng MW, Smyth MJ, Thomas DM. Translational biology of osteosarcoma. *Nat Rev Cancer* 2014; **14**: 722–35.

5 Porter DE, Holden ST, Steel CM, Cohen BB, Wallace MR, Reid R. A significant proportion of patients with osteosarcoma may belong to Li-Fraumeni cancer families. *J Bone Jt Surg Br Volume* 1992; **74**: 883–6.

6 Bougeard G, Renaux-Petel M, Flaman J-M, Charbonnier C, Fermey P, Belotti M *et al.* Revisiting Li-Fraumeni Syndrome From TP53 Mutation Carriers. *J Clin Oncol* 2015; **33**: 2345–2352.

7 Chen X, Bahrami A, Pappo A, Easton J, Dalton J, Hedlund E *et al.* Recurrent somatic structural variations contribute to tumorigenesis in pediatric osteosarcoma. *Cell Reports* 2014; **7**: 104–12.

8 Walkley CR, Qudsi R, Sankaran VG, Perry JA, Gostissa M, Roth SI *et al.* Conditional mouse osteosarcoma, dependent on p53 loss and potentiated by loss of Rb, mimics the human disease. *Gene Dev* 2008; **22**: 1662–76.

9 Berman SD, Calo E, Landman AS, Danielian PS, Miller ES, West JC *et al.* Metastatic osteosarcoma induced by inactivation of Rb and p53 in the osteoblast lineage. *Proc National Acad Sci* 2008; **105**: 11851–11856.

10 Lee TI, Young RA. Transcriptional Regulation and Its Misregulation in Disease. *Cell* 2013; **152**: 1237–1251.

11 Grigoriadis A, Schellander K, Wang Z, Wagner E. Osteoblasts are target cells for transformation in c-fos transgenic mice. *J Cell Biology* 1993; **122**: 685–701.

12 Gamberi G, Benassi MS, Bohling T, Ragazzini P, Molendini L, Sollazzo MR *et al.* C-myc and c-fos in Human Osteosarcoma: Prognostic Value of mRNA and Protein Expression. *Oncology* 1998; **55**: 556–563.

13 Ito Y, Bae S-C, Chuang LSH. The RUNX family: developmental regulators in cancer. *Nat Rev Cancer* 2015; **15**: 81–95.

14 Levanon D, Groner Y. Structure and regulated expression of mammalian RUNX genes. *Oncogene* 2004; **23**: 4211–4219.

15 Bauer O, Sharir A, Kimura A, Hantisteanu S, Takeda S, Groner Y. Loss of Osteoblast Runx3 Produces Severe Congenital Osteopenia. *Mol Cell Biol* 2015; **35**: 1097–1109.

16 Komori T, Yagi H, Nomura S, Yamaguchi A, Sasaki K, Deguchi K *et al.* Targeted Disruption of Cbfa1 Results in a Complete Lack of Bone Formation owing to Maturational Arrest of Osteoblasts. *Cell* 1997; **89**: 755–764.

17 Jain M, Arvanitis C, Chu K, Dewey W, Leonhardt E, Trinh M *et al.* Sustained Loss of a Neoplastic Phenotype by Brief Inactivation of MYC. *Science* 2002; **297**: 102–104.

18 Gilbert LA, Larson MH, Morsut L, Liu Z, Brar GA, Torres SE *et al.* CRISPR-Mediated Modular RNA-Guided Regulation of Transcription in Eukaryotes. *Cell* 2013; **154**: 442–451.

19 Pulikkan JA, Hegde M, Ahmad HM, Belaghzal H, Illendula A, Yu J *et al.* CBFβ-SMMHC Inhibition Triggers Apoptosis by Disrupting MYC Chromatin Dynamics in Acute Myeloid Leukemia. *Cell* 2018; **174**: 172-186.e21.

20 Cho SW, Xu J, Sun R, Mumbach MR, Carter AC, Chen YG *et al.* Promoter of lncRNA Gene PVT1 Is a Tumor-Suppressor DNA Boundary Element. *Cell* 2018; **173**: 1398-1412.e22.

21 Wierstra I, Alves J. The c- myc Promoter: Still MysterY and Challenge. *Adv Cancer Res* 2008; **99**: 113–333.

22 Cunningham L, Finckbeiner S, Hyde RK, Southall N, Marugan J, Yedavalli VRK *et al.* Identification of benzodiazepine Ro5-3335 as an inhibitor of CBF leukemia through quantitative high throughput screen against RUNX1–CBFβ interaction. *Proc National Acad Sci* 2012; **109**: 14592–14597.

23 Illendula A, Gilmour J, Grembecka J, Tirumala VSS, Boulton A, Kuntimaddi A *et al.* Small Molecule Inhibitor of CBFβ-RUNX Binding for RUNX Transcription Factor Driven Cancers. *Ebiomedicine* 2016; **8**: 117–131.

24 Ottaviano L, Schaefer K, Gajewski M, Huckenbeck W, Baldus S, Rogel U *et al.* Molecular characterization of commonly used cell lines for bone tumor research: A trans-European EuroBoNet effort. *Genes Chromosomes Cancer* 2010; **49**: 40–51.

25 Yamada C, Ozaki T, Ando K, Suenaga Y, Inoue K, Ito Y *et al.* RUNX3 Modulates DNA Damage-mediated Phosphorylation of Tumor Suppressor p53 at Ser-15 and Acts as a Co-activator for p53. *J Biol Chem* 2010; **285**: 16693–16703.

26 Martin JW, Zielenska M, Stein GS, Wijnen AJ van, Squire JA. The Role of RUNX2 in Osteosarcoma Oncogenesis. *Sarcoma* 2010; **2011**: 282745.

27 Shin MH, He Y, Marrogi E, Piperdi S, Ren L, Khanna C *et al.* A RUNX2-Mediated Epigenetic Regulation of the Survival of p53 Defective Cancer Cells. *Plos Genet* 2016; **12**: e1005884.

28 Deen M van der, Akech J, Lapointe D, Gupta S, Young DW, Montecino MA *et al.* Genomic Promoter Occupancy of Runt-related Transcription Factor RUNX2 in Osteosarcoma Cells Identifies Genes Involved in Cell Adhesion and Motility*. *J Biol Chem* 2012; **287**: 4503–4517.

29 He Y, Castro LF de, Shin MH, Dubois W, Yang HH, Jiang S *et al.* p53 Loss Increases the Osteogenic Differentiation of Bone Marrow Stromal Cells. *Stem Cells* 2015; **33**: 1304–1319.

30 Whittle MC, Izeradjene K, Rani PG, Feng L, Carlson MA, DelGiorno KE *et al.* RUNX3 Controls a Metastatic Switch in Pancreatic Ductal Adenocarcinoma. *Cell* 2015; **161**: 1345–60.

31 Walz S, Lorenzin F, Morton J, Wiese KE, Eyss B von, Herold S *et al.* Activation and repression by oncogenic MYC shape tumour-specific gene expression profiles. *Nature* 2014; **511**: 483–487.

32 Hosoi H, Niibori-Nambu A, Nah GSS, Bahirvani AG, Mok MMH, Sanda T *et al.* Super-enhancers for RUNX3 are required for cell proliferation in EBV-infected B cell lines. *Gene* 2021; **774**: 145421.

33 Li Q-L, Ito K, Sakakura C, Fukamachi H, Inoue K, Chi X-Z *et al.* Causal Relationship between the Loss of RUNX3 Expression and Gastric Cancer. *Cell* 2002; **109**: 113–124.

34 Ito K, Liu Q, Salto-Tellez M, Yano T, Tada K, Ida H *et al.* RUNX3, A Novel Tumor Suppressor, Is Frequently Inactivated in Gastric Cancer by Protein Mislocalization. *Cancer Res* 2005; **65**: 7743–7750.

35 Chuang LSH, Ito K, Ito Y. RUNX Proteins in Development and Cancer. *Adv Exp Med Biol* 2017; **962**: 299–320.

36 Bledsoe KL, McGee- Lawrence ME, Camilleri ET, Wang X, Riester SM, Wijnen AJ van *et al.* RUNX3 Facilitates Growth of Ewing Sarcoma Cells. *J Cell Physiol* 2014; **229**: 2049–2056.

37 Bushweller JH. Targeting transcription factors in cancer — from undruggable to reality. *Nat Rev Cancer* 2019; **19**: 611–624.

38 Morita K, Suzuki K, Maeda S, Matsuo A, Mitsuda Y, Tokushige C *et al.* Genetic regulation of the RUNX transcription factor family has antitumor effects. *J Clin Invest* 2017; **127**: 2815–2828.

39 Date Y, Ito K. Oncogenic RUNX3: A Link between p53 Deficiency and MYC Dysregulation. *Mol Cells* 2020; **43**: 176–181.

40 Gabay M, Li Y, Felsher DW. MYC Activation Is a Hallmark of Cancer Initiation and Maintenance. *Csh Perspect Med* 2014; **4**: a014241.

41 Lancho O, Herranz D. The MYC Enhancer-ome: Long-Range Transcriptional Regulation of MYC in Cancer. *Trends Cancer* 2018; **4**: 810–822.

42 Chuang LSH, Ito K, Ito Y. RUNX family: Regulation and diversification of roles through interacting proteins. *Int J Cancer* 2013; **132**: 1260–1271.

43 Sabapathy K, Lane DP. Therapeutic targeting of p53: all mutants are equal, but some mutants are more equal than others. *Nat Rev Clin Oncol* 2018; **15**: 13–30.

44 Taniuchi I, Osato M, Egawa T, Sunshine MJ, Bae S-C, Komori T *et al.* Differential Requirements for Runx Proteins in CD4 Repression and Epigenetic Silencing during T Lymphocyte Development. *Cell* 2002; **111**: 621–633.

45 Qin X, Jiang Q, Nagano K, Moriishi T, Miyazaki T, Komori H *et al.* Runx2 is essential for the transdifferentiation of chondrocytes into osteoblasts. *Plos Genet* 2020; **16**: e1009169.

46 Naoe Y, Setoguchi R, Akiyama K, Muroi S, Kuroda M, Hatam F *et al.* Repression of interleukin-4 in T helper type 1 cells by Runx/Cbfβ binding to the Il4 silencer. *J Exp Medicine* 2007; **204**: 1749–1755.

47 Jonkers J, Meuwissen R, Gulden H van der, Peterse H, Valk M van der, Berns A. Synergistic tumor suppressor activity of BRCA2 and p53 in a conditional mouse model for breast cancer. *Nat Genet* 2001; **29**: 418–425.

48 Alboran IM de, O'Hagan RC, Gärtner F, Malynn B, Davidson L, Rickert R *et al.* Analysis of C-MYC Function in Normal Cells via Conditional Gene-Targeted Mutation. *Immunity* 2001; **14**: 45–55.

49 Buenrostro JD, Wu B, Chang HY, Greenleaf WJ. ATAC-seq: A Method for Assaying Chromatin Accessibility Genome-Wide. *Current protocols in molecular biology* 2015; **109**: 21.29.1–9.

50 Chen S, Zhou Y, Chen Y, Gu J. fastp: an ultra-fast all-in-one FASTQ preprocessor. *Bioinformatics* 2018; **34**: i884–i890.

51 Langmead B, Salzberg SL. Fast gapped-read alignment with Bowtie 2. *Nat Methods* 2012; **9**: 357–359.

52 Heinz S, Benner C, Spann N, Bertolino E, Lin YC, Laslo P *et al.* Simple combinations of lineage-determining transcription factors prime cis-regulatory elements required for macrophage and B cell identities. *Molecular cell* 2010; **38**: 576–589.

53 Ramírez F, Ryan DP, Grüning B, Bhardwaj V, Kilpert F, Richter AS *et al.* deepTools2: a next generation web server for deep-sequencing data analysis. *Nucleic Acids Research* 2016; **44**: W160-5.

54 Bonev B, Cohen NM, Szabo Q, Fritsch L, Papadopoulos GL, Lubling Y *et al.* Multiscale 3D Genome Rewiring during Mouse Neural Development. *Cell* 2017; **171**: 557-572.e24.

Figure Legends

Figure 1. Runx3 is highly upregulated and oncogenic in *p53*-deficient OS.

(A) Heatmap representing color-coded expression levels of the top 10 highest-expressed TFs and the RUNX family genes across 86 OS patients harboring genetic alterations in *TP53*, *RB1*, *CDKN2A*, *ATRX*, and *MDM2*. The ratio of gene expression level in OS vs. normal osteoblasts (OB) is shown as $\log_2$FC. (B) Heatmap of the top 10 highest-expressed TFs and the Runx family genes in OS in seven *OS* mice. Seven TFs common to both human and mouse are shown in blue (A and B). (C) Levels of the indicated proteins in BM-MSCs, as determined by western blotting. (D) Survival of *Runx3$^{+/+}$*, *Runx3$^{fl/+}$*, and *Runx3(P1)$^{\Delta/\Delta}$* mice in the *OS* background, alongside Cre-free controls. (E) Incidence of OS in the indicated genotypes within 1 year and throughout the lifespan.

Figure 2. Myc is a positive target of Runx3 in *p53*-deficient OS.

(A) Heatmaps showing genome-wide occupancy of Runx3, H3K27ac, and open chromatin (ATAC-seq). Regions (y-axis) were divided into three clusters, each ordered by merged signal intensity for all profiles. Myc regulatory regions (red) were most frequently observed among the 1,624 strongly co-occupied regions. (B) Volcano plot of the changes in gene expression upon Runx3(P1) deletion in BM-MSCs of *OS* mice. BM-MSCs from *OS* (WT; n=4) and *OS*; *Runx3(P1)$^{\Delta/\Delta}$* (*Runx3(P1)$^{\Delta/\Delta}$*; n=5) mice were subjected to microarray analysis. Myc was one of the 1,552 genes (orange) significantly upregulated by Runx3(P1) in the absence of p53 ($p < 0.05$). (C) MYC/Myc expression levels plotted against RUNXs/Runxs expression levels in human (n=86, Fig. 1A) and mouse (n=24) OS. Spearman rank correlation coefficient is shown in each panel. (D) Survival of *Myc$^{+/+}$*and *Myc$^{fl/+}$* mice in the *OS* background, alongside Cre-free controls. (E) OS incidence of each mouse line within 1 year and throughout the lifespan. The cohort of *OS* mice is identical to that in Fig. 1D, E (D and E).

Figure 3. mR1 is a responsible element of Myc upregulation by Runx3.

(A) Profiles of Runx3 and open/active chromatin (ATAC and H3K27ac) in mOS1-1 cells, together with the homology score (PhyloP), are aligned across the 3-Mb Myc TAD. Target regions of CRISPRi are shown in gray. (B) Relative expression of *Myc* and *Pvt1* in mOS1-1 cells in which the indicated regions were targeted by dCas9-KRAB. Scrambled (Scr) sgRNA served as a control. Data are means ± SD (n=3). [**]$p < 0.01$; [*]$p < 0.05$. (C) Levels of the indicated proteins in each CRISPRi mOS1-1 clone, as determined by western blotting. (D) Schematic representing mR1, mR2, and mR3 in the *Myc* promoter, with associated profiles for ChIP-seq (Runx3 and H3K27ac) and ATAC-seq. (E) Levels of the indicated proteins in CRISPRi mOS1-1 cells in which the indicated regions were targeted by dCas9-KRAB, as determined by western blotting. (F) Tumorigenicity of each CRISPRi mOS1-1 cells. (G) Sequence alignments of mOS1-1 clones with either 1 bp (T7) or 3 bp (T13) homozygous deletion in mR1, together with a non-targeted control (Scr). (*H*) EMSA performed using nuclear extract of mOS1-1 cells and labeled DNA probes with either intact (WT) or mutated (T7 or T13) mR1, corresponding to the sequences shown in (G). Specificity of probe-bound Runx2 or Runx3 is demonstrated in Supplemental Fig. 12E. (I) Levels of the indicated proteins in each genome-edited mOS1-1 clone, as determined by western blotting. (J) Tumorigenicity of each genome-edited mOS1-1 clone. (K) Occupancy of RNA polymerase II on the indicated positions of the *Myc* regulatory region, with positive (*Gapdh*) and negative (gene desert) controls, as revealed by ChIP in Scr and T13 mOS1-1 cells. Data are means ± SD (n=3).

Figure 4. mR1 and Runx3 are responsible for development of OS in *p53*-deficient mice. (A) Levels of the indicated proteins in BM-MSCs from two individuals of each mouse line, as determined by western blotting. (B) Survival of the indicated genotypes. (C) Incidence of OS in the indicated genotypes within 1 year and throughout the lifespan. The results of *OS* mice are identical to those in Fig. 1D or E, and those of *OS*; *mR1*[m/m] and *OS*; *mR2*[m/m] mice are from two independent lines, each shown in Supplementary Fig. 10F, G, J, K (B and C). (D) Comparison of survival of *OS* mouse lines shown in Fig. 1D, 2D and (B): *OS*, *OS*; *Runx3*^{fl/+}, *OS*; *mR1*[m/m], *OS*; *Runx3(P1)*[Δ/Δ], and *OS*; *Myc*^{fl/+}. (*E*) Comparison of OS

incidence in *OS* mouse lines shown in (D) within 1 year and throughout the lifespan. (F) Survival of *OS* mice treated with or without (w/o) Ro5-3335 or AI-10-104 after the onset of OS.

Figure 5. Myc induction by Runx3 is dependent on *p53*-deficiency.

(A) Levels of the indicated proteins in BM-MSCs from two individuals of each mouse line, *OS* (p53$^{\Delta/\Delta}$), wild-type (WT), or *mR1*$^{m/m}$ (mR1$^{m/m}$), as determined by western blotting. (B) Levels of the indicated proteins in BM-MSCs from two individuals of each mouse line [WT, *Runx3(P1)*$^{\Delta/\Delta}$ (Runx3(P1)$^{\Delta/\Delta}$), p53$^{\Delta/\Delta}$, or *OS*;*Runx3(P1)*$^{\Delta/\Delta}$ (p53$^{\Delta/\Delta}$Runx3(P1)$^{\Delta/\Delta}$) mice], as determined by western blotting. (C) Levels of the indicated proteins in p53$^{\Delta/\Delta}$ or p53$^{\Delta/\Delta}$Runx3(P1)$^{\Delta/\Delta}$ BM-MSCs with or without exogenously restored p53, as determined by western blotting. (D) Levels of the indicated proteins in mOS1-1 cells expressing either WT or mutant p53 (R156P, R273H). Expression of p21 confirmed WT p53 function. (E) Co-immunoprecipitation of endogenous Runx3 and exogenous WT, R156P, or R273H p53 in mOS1-1 cells. Levels of the indicated proteins in immunoprecipitates obtained using anti-Runx3 antibody were determined by western blotting. (F) Effect of WT, R156P, or R273H p53 on RUNX3 transcriptional activity in *p53-* and *RUNX3*-negative G292 cells (n=3). (G) Efficacy of AI-10-104 (0, 0.2, 0.6, or 1.8 μM for 24 hours) on Myc expression in *p53*-negative mOS2-2 cells and *p53*-positive ST2 cells. (H) In normal cells, p53 attenuates Runx3 transactivation, whereas in OS, Runx3 aberrantly upregulates Myc in the absence of p53 or in the presence of mutant p53.
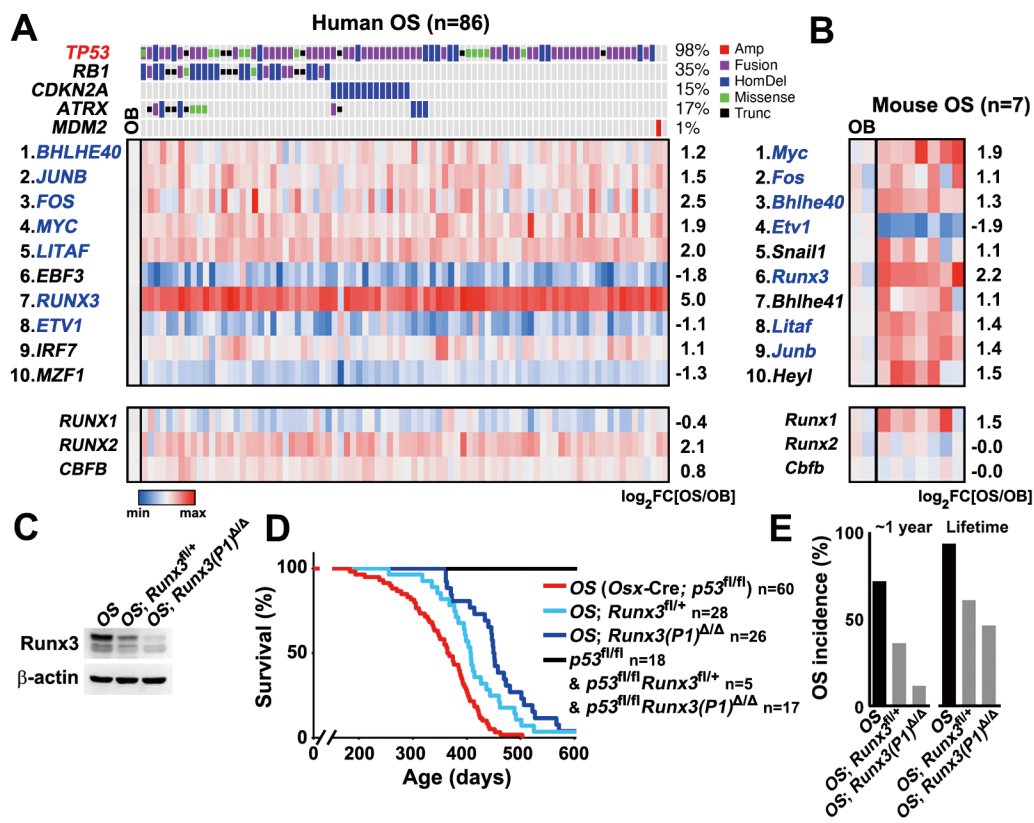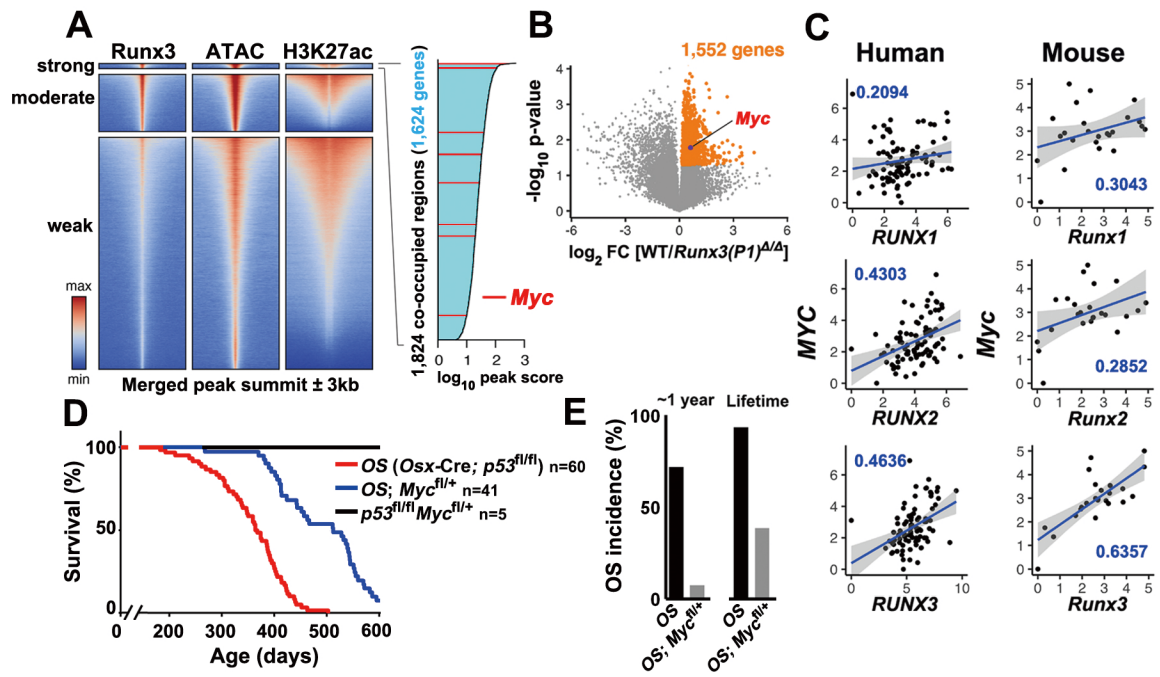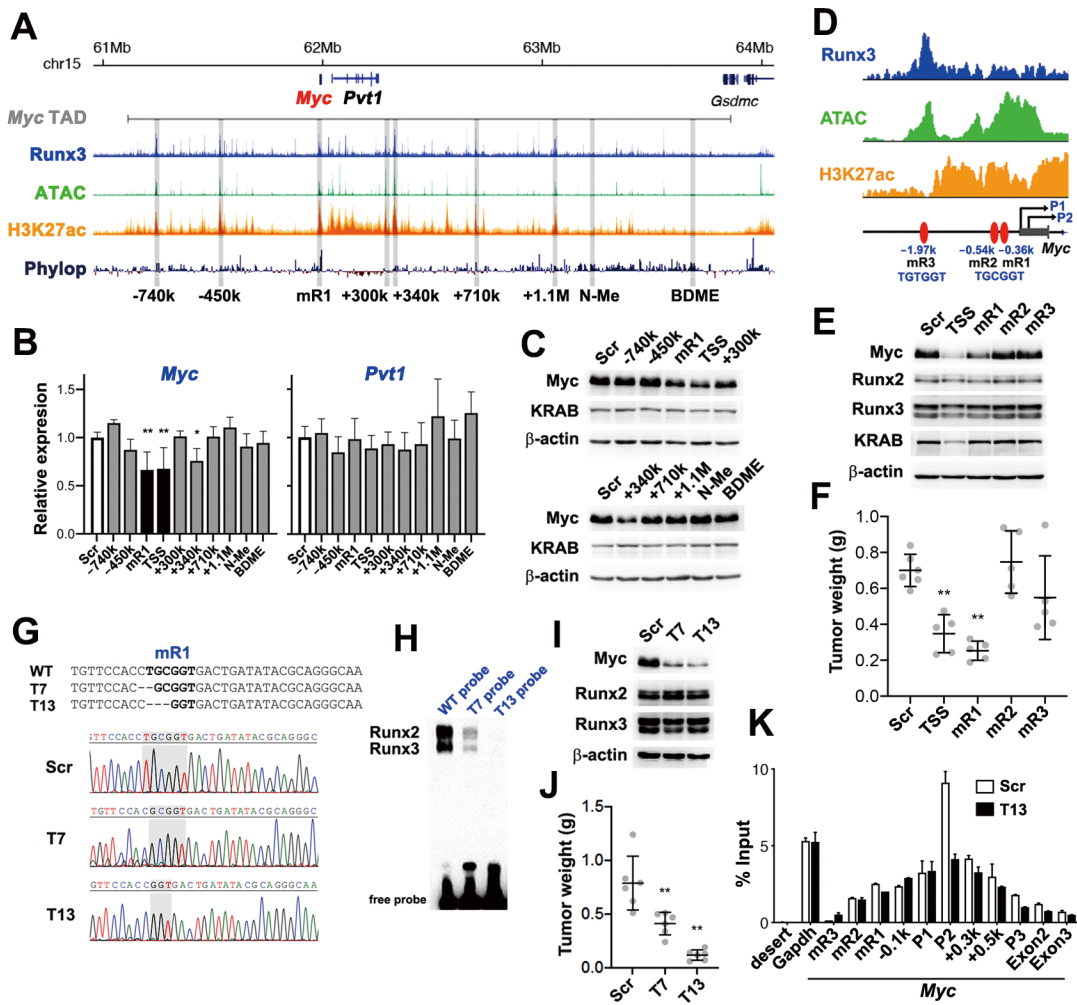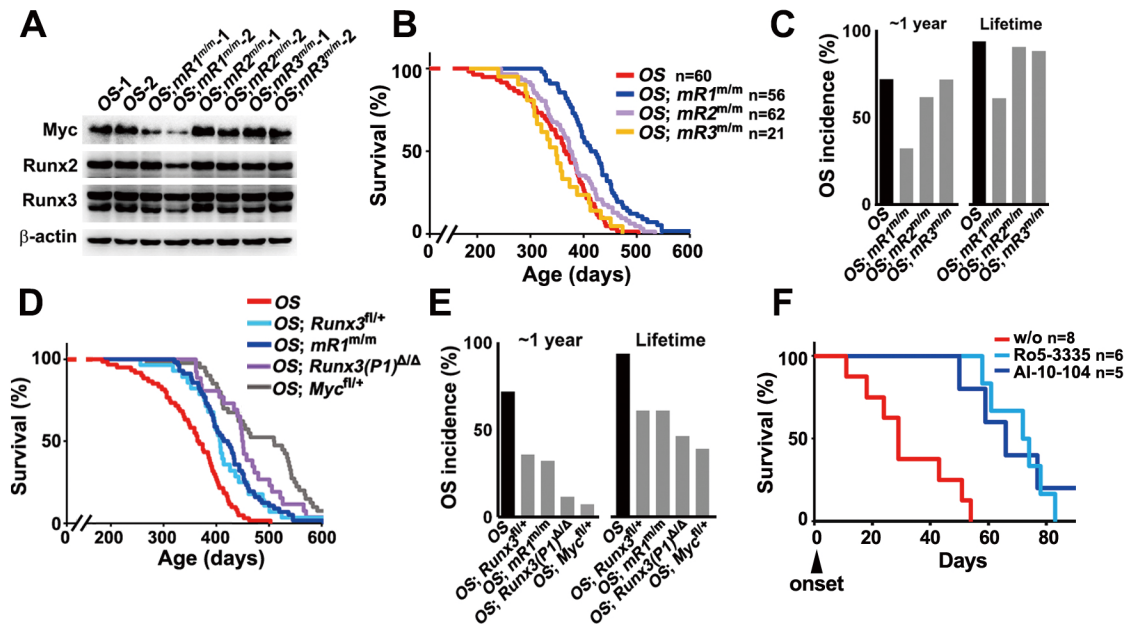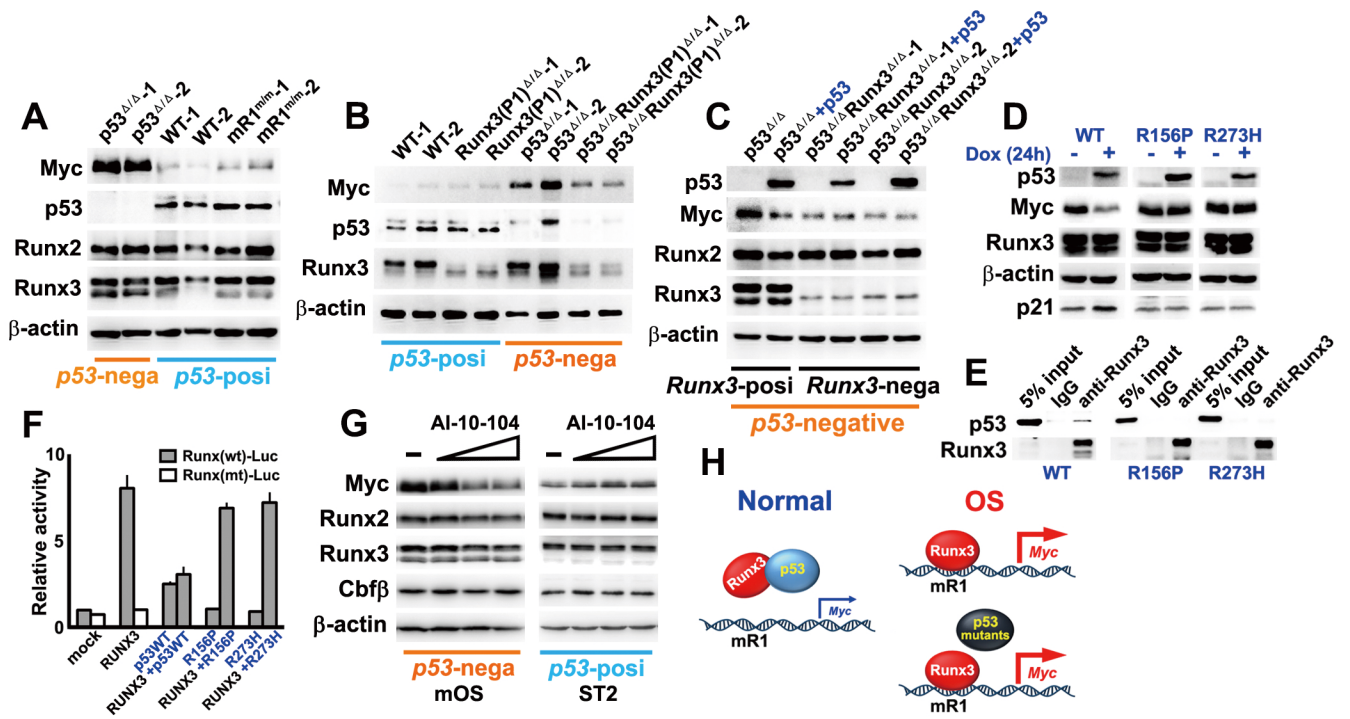
Figure 1

Figure 2

Figure 3

Figure 4

Figure 5